



**HAL**  
open science

# One-dimensional Model of Oxygen Transport Impedance Accounting for Convection Perpendicular to the Electrode

J. Mainka, G. Maranzana, A. Thomas, J. Dillet, S. Didierjean, O. Lottin

► **To cite this version:**

J. Mainka, G. Maranzana, A. Thomas, J. Dillet, S. Didierjean, et al.. One-dimensional Model of Oxygen Transport Impedance Accounting for Convection Perpendicular to the Electrode. *Fuel Cells*, 2012, 12 (5), pp.848 - 861. 10.1002/fuce.201100193 . hal-01486130

**HAL Id: hal-01486130**

**<https://hal.univ-lorraine.fr/hal-01486130>**

Submitted on 18 Dec 2023

**HAL** is a multi-disciplinary open access archive for the deposit and dissemination of scientific research documents, whether they are published or not. The documents may come from teaching and research institutions in France or abroad, or from public or private research centers.

L'archive ouverte pluridisciplinaire **HAL**, est destinée au dépôt et à la diffusion de documents scientifiques de niveau recherche, publiés ou non, émanant des établissements d'enseignement et de recherche français ou étrangers, des laboratoires publics ou privés.



## One-dimensional Model of Oxygen Transport Impedance Accounting for Convection Perpendicular to the Electrode

Journal:	<i>Fuel Cells</i>
Manuscript ID:	Draft
Wiley - Manuscript type:	Original Research Paper
Date Submitted by the Author:	n/a
Complete List of Authors:	Mainka, Julia; LNCC, CMC - 6097; LEMTA - INPL - UMR CNRS 7563, Pile à Combustible Maranzana, Gaël; LEMTA-INPL-UMR CNRS 7563, Pile à Combustible Thomas, Anthony; LEMTA-INPL-UMR CNRS 7563, Pile à Combustible Dillet, Jérôme; LEMTA-INPL-UMR CNRS 7563, Pile à Combustible Didierjean, Sophie; LEMTA-INPL-UMR CNRS 7563, Pile à Combustible Lottin, Olivier; LEMTA-INPL-UMR CNRS 7563, Pile à Combustible
Keywords:	Cathode, Modelling, Electrochemical Impedance Spectroscopy, PEMFC, Numerical Simulation

SCHOLARONE™  
Manuscripts

Review

# One-dimensional Model of Oxygen Transport Impedance Accounting for Convection Perpendicular to the Electrode

J. Mainka<sup>\*1,2</sup>, G. Maranzana<sup>2</sup>, A. Thomas<sup>2</sup>, J. Dillet<sup>2</sup>, S. Didierjean<sup>2</sup>, O. Lottin<sup>2</sup>

<sup>1</sup> Laboratório Nacional de Computação Científica (LNCC), CMC 6097, Av. Getúlio Vargas 333, 25651-075 Petrópolis, RJ, Caixa Postal 95113, Brazil

<sup>2</sup> Laboratoire d'Energétique et de Mécanique Théorique et Appliquée (LEMTA), UMR 7563 CNRS-INPL-UHP, 2, avenue de la Forêt de Haye, BP 160, 54504 Vandoeuvre-lès-Nancy Cedex, France

[\*] Corresponding Author, mainka@lncc.br

## Abstract

A one-dimensional model of oxygen transport in the diffusion media of Proton Exchange Membrane Fuel Cells (PEMFC) is presented, which considers convection perpendicular to the electrode in addition to diffusion. The resulting analytical expression of the convecto-diffusive impedance is obtained using a convection-diffusion equation instead of a diffusion equation in the case of classical Warburg impedance. The main hypothesis of the model is that the convective flux is generated by the evacuation of water produced at the cathode which flows through the porous media in vapor phase. This allows the expression of the velocity of the convective flux as a function of the current density and of the water transport coefficient  $\alpha$  (the fraction of water that is evacuated at the cathode outlet). Although the resulting expression of the oxygen transport impedance is not necessarily valid in all cases it enables us to estimate the impact of convection perpendicular to the electrode on PEMFC impedance spectra and to determine in which conditions the approximation by a purely diffusive oxygen transport is valid. Experimental observations confirm the numerical results.

**Keywords:** Cathode, Modeling, Electrochemical Impedance Spectroscopy, Parameter Estimation, PEMFC

## 1 Introduction

Applied to fuel cells, Electrochemical Impedance Spectroscopy (EIS) is a powerful diagnosis tool that can be used during operation with minimal perturbations [1--3]. A common application of this technique is the identification of the factors which limit the cell performance, i.e. ohmic conduction, charge separation and transfer and mass transport [1, 2, 4--7] and the dual objectives of improving the design of the membrane-electrode assembly (MEA) [8] and determining optimal working conditions [1, 9]. Appropriate models are required to discriminate between the different contributions to the cell impedance.

This work focuses on the analysis of the oxygen transport processes occurring at the cathode of H<sub>2</sub>/air fed Polymer Electrolyte Membrane Fuel Cells (PEMFC). PEMFC must be able to operate at high current densities with a satisfactory level of efficiency. Under these conditions, the slow oxygen diffusion to the active sites of the cathode has a direct influence on the oxygen reduction reaction (ORR). Consequently, a multitude of studies have focused on the derivation of an expression of the oxygen transport impedance, in order to achieve a better understanding of mass transport at the cathode [10--17].

Impedance spectra of air fed PEMFC usually show two loops in a frequency range between 10<sup>-3</sup> Hz and 10<sup>-5</sup> Hz [1, 7, 18]: one at high frequencies which is commonly attributed to charge transfer and capacitive processes in the electrodes and one at low frequencies associated with oxygen transport through the diffusive media. Various works highlight the limiting role of the gas diffusion layer for oxygen diffusion [1, 19, 20], but the origin of the LF loop in PEMFC impedance spectra has yet to be fully determined. Some of the most common explanations found in past studies are: slow oxygen diffusion through the backing layers [1], back diffusion of water in the membrane [2] or diffusion of water in the catalyst layer [21]. In addition, the experimental investigations of Schneider et al. [13, 14] found that the AC measuring signal induces concentration oscillations that propagate along the gas channel and influence the impedance measurements downstream, especially at low frequencies.

Notwithstanding the variety of explanations of the origin of the LF loop, most of the oxygen transport impedance models [16, 17, 22--26], among which the commonly used Warburg model [27], are based on the assumption that mass transport from the inlet of the diffusion medium to the reaction sites at the electrode occurs by diffusion only, whereas this is not necessarily justifiable. Therefore in this study, our aim was to verify the validity of this hypothesis by developing a one-dimensional oxygen transport model that accounts for the presence of a convective flux perpendicular to the electrode in addition to diffusion.

The oxygen transport model and the resulting 1D convecto-diffusive impedance are derived in section 2. The convective flux is accounted for by the evacuation of the water produced at the cathode in vapor phase. It can thus be expressed as a function of a water transport coefficient  $\alpha$  [28]. In section 3, we present a numerical analysis of the impact of convection perpendicular to the electrode on the oxygen concentration, and

consequently, on the oxygen transport impedance as a function of the operating conditions. The numerical study is completed by experimental results (section 4) obtained from PEMFC impedance spectra measured at different current densities and for different values of the water transport coefficient. These investigations allow an estimation of the conditions for which oxygen transport through PEMFC diffusion media can be approached by a purely diffusive flux.

## 2 Model Development

A schematic representation of the geometry of the cathode is shown in Figure 1. The description is one-dimensional and the reaction sites are assumed to be located at a reaction interface at  $x = 0$ .

Since the slow oxygen reduction reaction (ORR) is the main factor limiting the electrical performance of a PEMFC, especially when it is fed with air [1, 22], voltage losses caused by the anode reaction (HOR) are neglected. The cell voltage is expressed as:

$$E_{cell}(t) = E_0 - R_{hf} j(t) - \eta_{act}(t) \quad (1)$$

where  $E_0$  denotes the open circuit voltage and  $R_{hf}$  an ohmic resistance accounting for the ionic resistance of the membrane as well as for the ionic and electronic resistances of the various MEA components (catalyst layer, GDL, flow field plates).  $\eta_{act}$  is the voltage loss resulting from oxygen depletion and from the finite reaction rate of the ORR. At usual current densities and in steady-state,  $\eta_{act}$  follows a Tafel law [29, 30]:

$$\eta_{act}(t) = b \ln \left[ \frac{j_f(t) c_{O_2}^*}{j_0 c_{O_2}(x=0, t)} \right] \quad (2)$$

in which  $b$  denotes the Tafel slope. For the sake of simplicity, it is assumed that  $\eta_{act}$  and  $j_f$  are positive.

The cell current density  $j(t)$  is the sum of the faradaic current density  $j_f(t)$  and of the capacitive current density  $j_c(t) = C_{dl} \partial \eta_{act} / \partial t$ :

$$j(t) = j_f(t) + C_{dl} \frac{\partial \eta_{act}}{\partial t} \quad (3)$$

where  $C_{dl}$  stands for the double-layer capacity of the cathode.

In terms of mass transport, the main model hypotheses are the same as those leading to the expression of the finite Warburg impedance [27, 30]:

- The fuel cell is isothermal and isobaric.
- The oxygen transport is one-dimensional along the  $x$ -direction and assumed to only occur in the vapor phase.
- The oxygen concentration at the GDL/channel interface ( $x = \delta$ ) is constant in time.
- The active sites are situated at a reaction interface at  $x = 0$ .
- The diffusion through the pores of the active and backing layers is Fickian. By convention, the fluxes are considered positive in  $x$ -direction (from the membrane to the cathode). The  $O_2$  flux is considered with reference to the MEA flat surface ( $\approx A_{geom}$ ). The porosity  $\varepsilon$  of these layers is accounted for by the use of an effective diffusivity  $D^{eff}$  according to Archie's law [31, 32]:

$$D^{eff} = \varepsilon^m D \quad (4)$$

in which  $m$  is an exponent varying between 1.5 and 4 as a function of the orientation of the pores in the diffusion medium. The value of the binary diffusion coefficient  $D$  depends on the nature of diffusion. We studied the diffusion through the pores of the backing layers where the motion is governed by inter-particle collisions [33]:  $D$  is given by the molecular diffusion coefficient [34].

Contrary to the classical Warburg approach, we consider that the oxygen flux density  $N_{O_2}$  is the sum of a diffusive contribution  $J_{O_2}$  (which obeys the 1<sup>st</sup> Fick equation) and a convective contribution  $N_{O_2}^{conv}$ :

$$\begin{aligned} N_{O_2} &= J_{O_2} + N_{O_2}^{conv} \\ &= -D_{O_2}^{eff} \frac{dc_{O_2}}{dx} + c_{O_2} V \end{aligned} \quad (5)$$

It should be noted that strictly speaking, the diffusion of oxygen through the pores of the diffusion media of air fed PEMFC should be described by Maxwell-Stefan equations [34, 35]. But, no analytical solution of these equations in an oscillating regime exist, which is required for the derivation of an expression of the oxygen transport impedance. However, since the binary diffusion coefficients of  $O_2/H_2O$  and  $O_2/N_2$  are close to each other, one can reasonably describe the oxygen diffusion by the Fick equations.  $N_{O_2}^{conv}$  depends on the gas net velocity  $V$  which is assumed to be constant over the diffusion medium thickness. The total molar flux density  $N^{tot}$  through the cathode backing layer is expressed as:

$$N^{tot} = N_{O_2}^{conv} + N_{H_2O}^{GDL} = cV \quad \text{with} \quad c = c_{O_2} + c_{H_2O} \quad (6)$$

where  $N_{H_2O}^{GDL}$  denotes the flux of vapor passing through the cathode GDL. Note that one of the main model hypotheses is that all water passes through the GDL in vapor phase. The convective flux through the backing layers is assumed uniform (the possible condensation and evaporation of water is neglected). It can be expressed by the water transport coefficient  $\alpha$  which is defined as the ratio of the vapor flux through the GDL  $N_{H_2O}^{GDL}$  to that of the produced water  $N_{H_2O}^{prod} = j_f / 2F$ :

$$\alpha = \frac{N_{H_2O}^{GDL}}{N_{H_2O}^{prod}} \quad (7)$$

The total molar flux  $N^{tot}$  is null for  $\alpha = 0.5$ , i.e. when each mole of oxygen consumed by the fuel cell is replaced in the air channel by a mole of water vapor. This corresponds to a purely diffusive oxygen transport which is described by the classical Warburg approach [27]. In these conditions, and with the assumption that gases are ideal gases,  $V$  can be expressed as a function of  $\alpha$  and the faradaic current density  $j_f$ :

$$\begin{aligned} V &= \left( \alpha N_{H_2O}^{prod} + J_{O_2} \right) \frac{1}{c} \\ &= (2\alpha - 1) \frac{j_f}{4F} \frac{RT}{P} \end{aligned} \quad (8)$$

Consequently, the oxygen flux is described by a convection-diffusion equation of the form:

$$\frac{\partial c_{O_2}}{\partial t}(x, t) + V \frac{\partial c_{O_2}}{\partial x}(x, t) = D^{eff} \frac{\partial^2 c_{O_2}}{\partial x^2}(x, t) \quad (9)$$

The assumption of a reaction interface involves that  $N_{O_2} = -j_f/4F$ . Including this expression in Eq. (5) gives the boundary condition at the reaction interface ( $x = 0$ ):

$$-D^{eff} \frac{\partial c_{O_2}}{\partial x} \Big|_{x=0,t} + c_{O_2}(0, t) V = -\frac{j_f(t)}{4F} \quad (10)$$

The oxygen concentration at the interface of the diffusion medium with the air channel ( $x = \delta$ ) is equal to the equilibrium concentration:

$$c_{O_2}(\delta, t) = c_{O_2}^* \quad (11)$$

$$\text{with } c_{O_2}^* = 0.21 \times P / RT.$$

## 2.1 DC Solution

Solving Eq. (9) in steady-state gives the local oxygen concentration  $c_{O_2}(x)$ :

$$c_{O_2}(x) = A \exp\left(\frac{V}{D^{eff}} x\right) + B \quad (12)$$

The boundary condition at the membrane/electrode interface ( $x = 0$ ) (10) enables us to determine the integration constant B:

$$B = -\frac{j_f}{4FV} \quad (13)$$

and A can be deduced from the boundary condition at the gas channel/GDL interface ( $x = \delta$ ) (11):

$$\begin{aligned} c_{O_2}(\delta) = c_{O_2}^* &= A \exp\left(\frac{V}{D^{eff}} \delta\right) - \frac{j_f}{4FV} \\ \Rightarrow A &= \left( c_{O_2}^* + \frac{j_f}{4FV} \right) \exp\left(-\frac{V}{D^{eff}} \delta\right) \end{aligned} \quad (14)$$

Inserting (13) and (14) in the general expression of  $c_{O_2}(x)$  (12) yields finally:

$$c_{O_2}(x) = c_{O_2}^* \exp\left(-\frac{V\delta}{D^{eff}}\right) - \frac{j_f}{4FV} \left[ 1 - \exp\left(\frac{V}{D^{eff}}(x - \delta)\right) \right] \quad (15)$$

The oxygen concentration at the reaction interface in steady-state is thus given by:

$$c_{O_2}(0) = c_{O_2}^* \exp\left(-\frac{V\delta}{D^{eff}}\right) - \frac{j_f}{4FV} \left[ 1 - \exp\left(-\frac{V\delta}{D^{eff}}\right) \right] \quad (16)$$

If the convective flux velocity tends to zero ( $\alpha \rightarrow 0.5$ ), Eq. (16) tends to a linear expression describing oxygen transport by diffusion only:

$$\lim_{V \rightarrow 0} c_{O_2}(0) = c_{O_2}^* - \frac{j_f \delta}{4FD^{eff}} \quad (17)$$

## 2.2 AC Solution

The convection-diffusion Eq. (9) must be solved in the transient regime. In the case of harmonic oscillations of small amplitude, the system is assumed to remain linear. Consequently, each variable  $X$  ( $X = j_f, \eta_{act}, c_{O_2}, V$ ) can be decomposed into a steady-state  $\langle X \rangle_t$  and a sinusoidal component of amplitude  $\Delta \bar{X}$ , which leads to:

$$\begin{aligned} E_{cell}(t) &= \langle E_{cell} \rangle_t + \Delta \bar{E}_{cell} \exp(i\omega t) \\ j(t) &= \langle j \rangle_t + \Delta \bar{j} \exp(i\omega t) \\ j_f(t) &= \langle j_f \rangle_t + \Delta \bar{j}_f \exp(i\omega t) \\ \eta_{act}(t) &= \langle \eta_{act} \rangle_t + \Delta \bar{\eta}_{act} \exp(i\omega t) \\ c_{O_2}(x, t) &= \langle c_{O_2}(x) \rangle_t + \Delta \bar{c}_{O_2}(x) \exp(i\omega t) \\ V(t) &= \langle V \rangle_t + \Delta \bar{V} \exp(i\omega t) \end{aligned} \quad (18)$$

The cell impedance is defined by,  $Z_{cell} = -\Delta \bar{E}_{cell} / \Delta \bar{j}$ , and the amplitudes of the cell potential  $\Delta \bar{E}_{cell}$  and current density  $\Delta \bar{j}$  can be derived from Eq. (1)-(3). This leads to:

$$\begin{aligned} \Delta \bar{E}_{cell} &= -R_{hf} \Delta \bar{j} - \Delta \bar{\eta}_{act} \\ \Delta \bar{\eta}_{act} &= b \frac{\Delta \bar{j}_f}{\langle j_f \rangle_t} - b \frac{\Delta \bar{c}_{O_2}(0)}{\langle c_{O_2}(0) \rangle_t} \\ \Delta \bar{j} &= \Delta \bar{j}_f + i\omega C_{dl} \Delta \bar{\eta}_{act} \end{aligned} \quad (19)$$

Note that the mean value of the faradaic current density  $\langle j_f \rangle_t$  is equal to that of the total current density  $\langle j \rangle_t$  since the time-averaged capacitive current is zero,  $\langle j_c \rangle_t = C_{dl} \langle \partial \eta_{act} / \partial t \rangle_t = 0$ . The above expressions meant  $Z_{cell}$  can be written in an explicit form:

$$Z_{cell} = R_{hf} + \frac{1}{\frac{b}{\langle j_f \rangle_t} - \frac{b}{\langle c_{O_2}(0) \rangle_t} \frac{\Delta \bar{c}_{O_2}(0)}{\Delta \bar{j}_f} + i\omega C_{dl}} \quad (20)$$

In addition to a high frequency resistance  $R_{hf}$  and a double-layer capacity  $C_{dl}$ , the cell impedance depends on a charge transfer resistance  $R_{ct} = b / \langle j_f \rangle_t$  and an oxygen transport impedance

$$Z_{c_{O_2}} = -\frac{b}{\langle c_{O_2}(0) \rangle_t} \frac{\Delta \bar{c}_{O_2}(0)}{\Delta \bar{j}_f}. \text{ To obtain an explicit expression of } Z_{c_{O_2}}, \text{ the amplitude of the oxygen}$$

concentration at the reaction interface  $\Delta \bar{c}_{O_2}(0)$  has to be expressed as a function of the amplitude of the faradaic current density  $\Delta \bar{j}_f$ . This can be achieved by solving the convection-diffusion equation (9) in oscillating regime in the conditions of the convecto-diffusive oxygen transport model. Using the system of equations (18), the convection-diffusion equation (9) takes the form:

$$i\omega \Delta \bar{c}_{O_2}(x) e^{i\omega t} + (\langle V \rangle_t + \Delta \bar{V} e^{i\omega t}) \frac{\partial \Delta \bar{c}_{O_2}(x) e^{i\omega t}}{\partial x} = D^{eff} \frac{\partial^2 \Delta \bar{c}_{O_2}(x) e^{i\omega t}}{\partial x^2} \quad (21)$$

As the signal variations were of small amplitude (maximum 10% of their steady-state values), the terms of second order can be neglected so that Eq. (21) reduces to:

$$i\omega \Delta \bar{c}_{O_2}(x) + \langle V \rangle_t \frac{\partial \Delta \bar{c}_{O_2}(x)}{\partial x} = D^{eff} \frac{\partial^2 \Delta \bar{c}_{O_2}(x)}{\partial x^2} \quad (22)$$

The general solution of (22) is:

$$\Delta \bar{c}_{O_2}(x) = A \exp(r_1 x) + B \exp(r_2 x) \quad (23)$$

with

$$r_1 = \frac{\langle V \rangle_t}{2D^{eff}} + \sqrt{\left(\frac{\langle V \rangle_t}{2D^{eff}}\right)^2 + \frac{i\omega}{D^{eff}}} \quad (24)$$

$$r_2 = \frac{\langle V \rangle_t}{2D^{eff}} - \sqrt{\left(\frac{\langle V \rangle_t}{2D^{eff}}\right)^2 + \frac{i\omega}{D^{eff}}} \quad (25)$$

Similarly, the boundary condition at the reaction interface (10) takes the form:

$$-D^{eff} \frac{\partial \Delta \bar{c}_{O_2}}{\partial x} \Big|_{x=0} + \langle V \rangle_t \Delta \bar{c}_{O_2}(0) + \Delta \bar{V} \langle c_{O_2}(0) \rangle_t = -\frac{\Delta \bar{j}_f}{4F} \quad (26)$$

where  $\langle c_{O_2}(0) \rangle_t$  is given by (16). The oxygen concentration at the GDL/channel interface is assumed constant, which leads to:  $\Delta \bar{c}_{O_2}(\delta) = 0$ . The coefficients A and B can thus be determined with these two boundary conditions:

$$x=0: \quad r_1 A + r_2 B - \frac{\langle V \rangle_t}{D^{eff}} (A + B) = \left[ 1 + (2\alpha - 1) \frac{RT}{P} \langle c_{O_2}(0) \rangle_t \right] \frac{\Delta \bar{j}_f}{4FD^{eff}} \quad (27)$$

$$x=\delta: \quad A \exp(r_1 \delta) + B \exp(r_2 \delta) = 0 \quad (28)$$

$$\Rightarrow A = \frac{1 + (2\alpha - 1) \frac{RT}{P} \langle c_{O_2}(0) \rangle_t}{\left(r_1 - \frac{\langle V \rangle_t}{D^{eff}}\right) \exp(r_2 \delta) - \left(r_2 - \frac{\langle V \rangle_t}{D^{eff}}\right) \exp(r_1 \delta)} \exp(r_2 \delta) \frac{\Delta \bar{j}_f}{4FD^{eff}} \quad (29)$$

$$B = -\frac{1 + (2\alpha - 1) \frac{RT}{P} \langle c_{O_2}(0) \rangle_t}{\left(r_1 - \frac{\langle V \rangle_t}{D^{eff}}\right) \exp(r_2 \delta) - \left(r_2 - \frac{\langle V \rangle_t}{D^{eff}}\right) \exp(r_1 \delta)} \exp(r_1 \delta) \frac{\Delta \bar{j}_f}{4FD^{eff}} \quad (30)$$

Inserting (29) and (30) in (23) yields the explicit expression of the amplitude of oxygen concentration oscillations along the x-direction:

$$\Delta \bar{c}_{O_2}(x) = -\frac{\exp(r_1 \delta + r_2 x) - \exp(r_2 \delta + r_1 x)}{\left(r_1 - \frac{\langle V \rangle_t}{D^{eff}}\right) \exp(r_2 \delta) - \left(r_2 - \frac{\langle V \rangle_t}{D^{eff}}\right) \exp(r_1 \delta)} \left[ 1 + (2\alpha - 1) \frac{RT}{P} \langle c_{O_2}(0) \rangle_t \right] \frac{\Delta \bar{j}_f}{4FD^{eff}} \quad (31)$$

And at the electrode/membrane interface ( $x = 0$ ), replacing  $r_1$  and  $r_2$  by their respective expressions (Eq. (24) and Eq. (25)), gives:

$$\Delta \bar{c}_{O_2}(x) = -\frac{1 + (2\alpha - 1) \frac{RT}{P} \langle c_{O_2}(0) \rangle_t}{\frac{\sqrt{\left(\frac{\langle V \rangle_t}{2D^{eff}}\right)^2 + \frac{i\omega}{D^{eff}}}}{\tanh\left(\sqrt{\left(\frac{\langle V \rangle_t}{2D^{eff}}\right)^2 + \frac{i\omega}{D^{eff}}}\delta\right)} + \frac{\langle V \rangle_t}{2D^{eff}}} \frac{\Delta \bar{j}_f}{4FD^{eff}} \quad (32)$$

Hence, it is possible to express explicitly the convecto-diffusive oxygen transport impedance appearing in (20):

$$\begin{aligned}
Z_{conv,diff}^{1D} &= -\frac{b}{\langle c_{O_2}(0) \rangle_t} \frac{\Delta \bar{c}_{O_2}(0)}{\Delta \bar{j}_f} \\
&= \frac{b}{4FD^{eff} \langle c_{O_2}(0) \rangle_t} \frac{1 + (2\alpha - 1) \frac{RT}{P} \langle c_{O_2}(0) \rangle_t}{\sqrt{\left( \frac{\langle V \rangle_t}{2D^{eff}} \right)^2 + \frac{i\omega}{D^{eff}}} + \frac{\langle V \rangle_t}{2D^{eff}}} \\
&\quad \frac{1}{\tanh \left( \sqrt{\left( \frac{\langle V \rangle_t}{2D^{eff}} \right)^2 + \frac{i\omega}{D^{eff}}} \delta \right)} \quad (33)
\end{aligned}$$

In the absence of any convective flux ( $V = 0$ ,  $\alpha = 0.5$ ), Eq. (33) takes the form of the finite Warburg impedance  $Z_W$ :

$$Z_{conv,diff}^{1D} (V = 0, \alpha = 0.5) = Z_W = \frac{b}{4F \langle c_{O_2}(0) \rangle_t} \frac{\tanh \left( \sqrt{\frac{i\omega}{D^{eff}}} \delta \right)}{\sqrt{i\omega D^{eff}}} \quad (34)$$

In addition, the low frequency limit of the convecto-diffusive impedance can be derived from Eq. (33) as a function of  $\alpha$ , which leads to:

$$\lim_{\omega \rightarrow 0} Z_{conv,diff}^{1D} = \frac{b}{4FD^{eff} \langle c_{O_2}(0) \rangle_t} \frac{1 + (2\alpha - 1) \frac{RT}{P} \langle c_{O_2}(0) \rangle_t}{\frac{\langle V \rangle_t}{2D^{eff}} \left[ \frac{1}{\tanh \left( \frac{\langle V \rangle_t \delta}{2D^{eff}} \right)} + 1 \right]} \quad (35)$$

with  $V$  a function of the water transport coefficient  $\alpha$  (8). It is thus possible to express the low frequency limit of the cell impedance  $R_{if}^\alpha$  as a function of the convective flux velocity:

$$R_{if}^\alpha = \lim_{\omega \rightarrow 0} Z_{cell} = R_{hf} + R_{ct} + \lim_{\omega \rightarrow 0} Z_{conv,diff}^{1D}(\alpha) \quad (36)$$

which allows to estimate the impact of convection on the low frequency limit of PEMFC impedance spectra. It should be noted that in the case of a purely diffusive oxygen transport ( $\alpha = 0.5$  and  $\langle V \rangle_t = 0$ ) we have:

$$\lim_{\omega \rightarrow 0} Z_{conv,diff}^{1D}(\alpha = 0.5) = \lim_{\omega \rightarrow 0} Z_W = \frac{b}{4FD^{eff} \langle c_{O_2}^{\alpha=0.5}(0) \rangle_t} \quad (37)$$

where  $\langle c_{O_2}^{\alpha=0.5}(0) \rangle_t$  is given by Eq. (17).

### 3 Numerical Results

The numerical simulations are made in the conditions described in Table 1.

Three different cases were considered:

- $\alpha = 0$ : all water flows through the membrane and the convective flux is oriented in the same direction as the diffusive one.
- $\alpha = 0.5$ : only half of the water is evacuated through the cathode GDL. The convective flux is null and the oxygen transport occurs only by diffusion (assumption leading to the expression of the Warburg diffusion impedance (34)).
- $\alpha = 1$ : all water is evacuated through the cathode GDL and the convective flux is directed opposite to the diffusive flux.

#### 3.1 Impact of a convective flux on the oxygen concentration at the reaction interface

Figure 2 shows the evolution of the oxygen concentration at the reaction interface ( $x = 0$ ) normalized relative to the inlet concentration  $c_{O_2}(0) / c_{O_2}^*$  as a function of  $j_f^1$  in the operating conditions of Table 1.

As the curves in Figure 2 show, convection was found to have no significant influence on the concentration at the electrode at low current densities. However, the discrepancies between the three cases increase with  $j_f$ : when the convective flux is oriented in the same direction as diffusion ( $\alpha = 0$ ), the values of  $c_{O_2}(0)$  are higher. When the convective flux is oriented in the opposite direction ( $\alpha = 1$ ),  $c_{O_2}(0)$  is lower than in the purely diffusive case.

The relative error (in terms of  $O_2$  concentration) made when using Eq. (17) instead of (16) can be quantified by the ratio  $\Delta c_{O_2}^\alpha(0) / c_{O_2}^{\alpha=0.5}(0)$  with  $\Delta c_{O_2}^\alpha(0) = |c_{O_2}^{\alpha=0.5}(0) - c_{O_2}^\alpha(0)|$ . Figure 3 depicts the evolution of  $\Delta c_{O_2}^\alpha(0) / c_{O_2}^{\alpha=0.5}(0)$  as a function of the current density for  $\alpha = 0$  (black bars) and  $\alpha = 1$  (blue bars). One can see that up to a current density  $j_f = 0.5 \text{ Acm}^{-2}$ , the relative error does not exceed 10%. However,  $\Delta c_{O_2}^\alpha(0) / c_{O_2}^{\alpha=0.5}(0)$  increases sharply with the current density and reaches almost 80% for  $j_f = 1.2 \text{ Acm}^{-2}$  and  $\alpha = 0$ . It should also be noted that the relative error is more important for a convective flux oriented in the direction of diffusion ( $\alpha = 0$ ) than in the opposite direction ( $\alpha = 1$ ).

It is thus possible to define a criterion indicating whether the influence of convection on  $c_{O_2}(0)$  may be neglected or not according to the water transport coefficient (for example if the relative error is below 10%). Note that according to Colinart et al. [36] the experimental values of  $\alpha$  are frequently close to 0.5. Our numerical investigations show that even if  $\alpha = 0$  or 1,  $\Delta c_{O_2}^\alpha(0) / c_{O_2}^{\alpha=0.5}(0)$  remains below 10% up to a current density of about  $0.5 \text{ Acm}^{-2}$ . Consequently, the relative error is even lower when  $\alpha$  is close to 0.5. Thus, it can be assumed that, in common operating conditions of PEMFC, the effect of convection on the oxygen concentration is negligible in a first approximation.

## 3.2 Impact of a convective flux on PEMFC impedance spectra

In this section, the cell impedance is expressed by Eq. (20) where the oxygen transport impedance is given by the 1D convecto-diffusive impedance  $Z_{conv,diff}^{1D}$  (33). The values of the main parameters used for the simulations are given in Table 1 (in the reference case). The high frequency parameters were set to typical values estimated at  $j_{cell} = 0.5 \text{ Acm}^{-2}$  (cf. section 4), i.e.  $R_{hf} = 0.13 \Omega \text{ cm}^2$ ,  $R_{ct} = 0.19 \Omega \text{ cm}^2$  (which corresponds to  $b = 95 \text{ mV}$ ) and  $C_{dl} = 0.02 \text{ Fcm}^{-2}$ . The experimental observations show that these parameters did not vary significantly with the current density, therefore we consider them as constant for this study. The effective diffusion coefficient in the GDL is set to  $D^{eff} = 10^{-6} \text{ m}^2 \text{ s}^{-1}$  [34]. The impedance spectra were simulated for frequencies ranging between  $10^{-3}$  Hz and  $10^5$  Hz with a resolution of 10 points per decade. In order to test the effect of convection, we considered the same three values of the water transport coefficient as above:  $\alpha = 0, 0.5$ , and 1.

### 3.2.1 Impact of the high frequency parameters $C_{dl}$ and $R_{ct}$

Figure 4(a) and Figure 4(b) show impedance spectra simulated with different values of  $C_{dl}$  and  $R_{ct}$ : the values of  $C_{dl}$  range between  $0.002 \text{ Fcm}^{-2}$  and  $0.2 \text{ Fcm}^{-2}$  and those of  $R_{ct}$  between  $0.019 \Omega \text{ cm}^2$  and  $0.19 \Omega \text{ cm}^2$ . The other parameters were kept constant. For the highest values ( $C_{dl} = 0.2 \text{ Fcm}^{-2}$  and  $R_{ct} = 0.19 \Omega \text{ cm}^2$ ), the low frequency loop seemed to disappear and the spectra exhibited only one loop. This was actually due to the large high frequency loop (compared to the low frequency loop), which dominates the whole spectrum, all the more so since the diffusion coefficient is in the range of gas diffusion through the pores of the GDL in the absence of liquid water ( $D^{eff} = 10^{-6} \text{ m}^2 \text{ s}^{-1}$ ). The low frequency loop becomes visible when the values of  $R_{ct}$  and  $C_{dl}$  were significantly reduced, which shifts the capacitive loop to higher frequencies. This result complies well with previous findings in studies [11].

The curves in Figure 4 confirm that the presence of a convective flux perpendicular to the electrode affects the impedance spectra only in the low and intermediate frequency range ( $\nu < 100 \text{ Hz}$ ): a convective flux oriented in the direction opposite to the diffusive flux ( $\alpha = 1$ ) widens the LF loop, while a convective flux in the same direction ( $\alpha = 0$ ) reduces its size. The value of the double-layer capacity affects that of the frequency limit  $\nu_{lim}$  above which the effects of convection are negligible.  $\nu_{lim}$  increases when  $C_{dl}$  decreases. However, it does not seem to be a function of the charge transfer resistance  $R_{ct}$ . Furthermore, the impact of  $\alpha$  on the impedance does not depend on  $C_{dl}$  (Figure 4(a)).

This is not the case for the charge transfer resistance:  $R_{ct}$  depends on the oxygen concentration at the reaction interface through the current density ( $R_{ct} = b/j_f$ ). The impact of convection on the impedance varies thus with the value of  $R_{ct}$  (Figure 4(b)). It should be noted that in practice, the value of  $R_{ct}$  is affected by the presence of convection.

<sup>1</sup> To simplify the notations,  $j_f$  denotes in the following the time-averaged faradaic current density  $\langle j_f \rangle_t$  which is equivalent to the mean cell current density  $\langle j \rangle_t$ .

### 3.2.2 Impact of the diffusion parameters $D^{\text{eff}}$ and $\delta$

The impact of convection on the cell impedance depends on the ratio of convection (expressed by the mean gas velocity  $V$ ) to diffusion (characterized by the diffusion velocity defined by:  $V_{\text{diff}} = \delta/D^{\text{eff}}$ ). The convective flux velocity can be determined using Eq. (8). In the reference conditions of Table 1, we obtain:

$$|V| = 3.5 \cdot 10^{-4} \text{ ms}^{-1} \text{ in both limit cases } (\alpha = 0, 1)$$

$$V_{\text{diff}} = 5 \cdot 10^{-3} \text{ ms}^{-1}$$

$V_{\text{diff}}$  is about 10 times higher than  $V$ , showing that the oxygen transport is governed mostly by diffusion. For lower values of the diffusive flux velocity  $V_{\text{diff}}$ , when the convective flux remains unchanged, the impact of convection on the impedance spectra is more pronounced. This is reflected by the curves in Figure 5(a) and Figure 5(b): decreasing  $D^{\text{eff}}$  or increasing  $\delta$  results in an enlargement of the low frequency loop and simultaneously, in a stronger impact of  $\alpha$ .

The impact of convection on the **oxygen transport impedance** can be estimated by introducing the quantity  $\Delta Z_{c_{O_2}}^{\alpha}$  giving the difference between the low frequency limits of  $\Delta Z_{\text{conv,diff}}^{1D}$  (35) and  $Z_W$  (37) as a function of  $\alpha$ ,

normalized with reference to the LF limit of  $Z_W$ :

$$\Delta Z_{c_{O_2}}^{\alpha} = \lim_{\omega \rightarrow 0} \left| \frac{Z_W - Z_{\text{conv,diff}}^{\alpha}}{Z_W} \right|$$

$$= \left| 1 - \frac{\langle c_{O_2}^{\alpha=0.5}(0) \rangle_t \left[ 1 + (2\alpha - 1) \frac{RT}{P} \langle c_{O_2}(0) \rangle_t \right]}{\langle c_{O_2}(0) \rangle_t \left[ 1 + \frac{1}{\frac{\langle V \rangle_t}{2V_{\text{diff}}} \tanh\left(\frac{\langle V \rangle_t}{2V_{\text{diff}}}\right)} \right]} \right| \quad (38)$$

The impact of convection on the **cell impedance** can be quantified thanks to the low frequency resistance  $R_{lf}^{\alpha}$  (36) corresponding to the intercept of the spectra with the real axis.  $\Delta R_{lf}^{\alpha}$  stands for the normalized difference between  $R_{lf}^{\alpha}$  ( $\alpha = 0,1$ ) and the LF resistance in the case of a purely diffusive oxygen transport  $R_{lf}^{\alpha=0.5}$ :

$$\Delta R_{lf}^{\alpha} = \lim_{\omega \rightarrow 0} \left| \frac{R_{lf}^{\alpha=0.5} - R_{lf}^{\alpha}}{R_{lf}^{\alpha=0.5}} \right|$$

$$= \left| \frac{1}{1 + \frac{4FV_{\text{diff}} \langle c_{O_2}^{\alpha=0.5}(0) \rangle_t}{b} (R_{hf} + R_{ct})} \Delta Z_{c_{O_2}}^{\alpha} \right| \quad (39)$$

Table 2 shows the values of  $\Delta Z_{c_{O_2}}^{\alpha}$  and  $\Delta R_{lf}^{\alpha}$  calculated in the conditions of Table 1 for two different cases: first for the reference case  $V_{\text{diff}} = 5 \cdot 10^{-3} \text{ ms}^{-1}$  ( $D^{\text{eff}} = 10^{-6} \text{ m}^2 \text{ s}^{-1}$ ,  $\delta = 200 \text{ }\mu\text{m}$ ) and secondly with a diffusive flow velocity divided by 2 ( $V_{\text{diff}}/2 \leftrightarrow D^{\text{eff}} = 5 \cdot 10^{-7} \text{ m}^2 \text{ s}^{-1}$ ,  $\delta = 200 \text{ }\mu\text{m}$  or  $D^{\text{eff}} = 10^{-6} \text{ m}^2 \text{ s}^{-1}$ ,  $\delta = 400 \text{ }\mu\text{m}$ ).

This example shows that the impact of convection on impedance depends to a large extent on the diffusive flux velocity, more precisely it increases inversely to  $V_{\text{diff}}$ . However, even when the effects on the cell impedance are low ( $\Delta R_{lf}^{\alpha} \approx 4\%$ ), the oxygen transport impedance is significantly affected by the presence of a convective flux ( $\Delta Z_{c_{O_2}}^{\alpha} \approx 20\%$ ). Moreover, the impact of a convective flux is greater when it is oriented opposite to the diffusion ( $\alpha > 0.5$ ) than in the same direction ( $\alpha < 0.5$ ).

According to this model, there is a critical value of the diffusive flux velocity  $V_{diff}^{crit}$  function of  $j_f$  and  $\alpha$ , below which all oxygen stops reaching the reaction sites and its concentration at the reaction interface becomes null:  $c_{O_2}(x=0) = 0$ . As a consequence, the cell impedance tends toward infinity when the diffusion velocity approaches  $V_{diff}^{crit}$ . For  $\alpha \neq 0.5$ , the expression of the critical velocity can be deduced from Eq. (16). If  $\alpha = 0.5$ , the critical value is obtained with the expression of the oxygen concentration in the case of a purely diffusive flux (17) as follows:

$$\alpha \neq 0.5: V_{diff}^{crit} = \frac{D_{crit}^{eff}}{\delta_{crit}} = \frac{(2\alpha - 1) j_f RT}{4FP \ln(1 + 0.21(2\alpha - 1))} \quad (40)$$

$$\alpha = 0.5: V_{diff}^{crit} = \frac{D_{crit}^{eff}}{\delta_{crit}} = \frac{j_f}{4Fc_{O_2}^*} \quad (41)$$

As the diffusion is characterized by the effective diffusivity and the diffusion layer thickness, it is possible to determine the critical values of one of these parameters as a function of the others. The critical values determined in the conditions of the reference case (Table 1) are given in Table 3.

As expected, the value of  $V_{diff}^{crit}$  is lower for a convective flux directed in the direction of diffusion than a convective flux in the opposite direction. Nevertheless, the critical values are close to each other in the three cases.

### 3.2.3 Impact of the current density $j_f$

Equation (8) shows that  $V$  also depends on the current density  $j_f$ : the convective flux increases with  $j_f$  which explains its impact on the impedance spectra. Figure 6 depicts impedance spectra simulated in the operating conditions of Table 1 for three different current densities:  $j_f = 0.5 \text{ Acm}^{-2}$ ,  $j_f = 1 \text{ Acm}^{-2}$  and  $j_f = 1.3 \text{ Acm}^{-2}$ . Clearly the impact of convection on the impedance spectra increases significantly with the current density. At  $j_f = 1.3 \text{ Acm}^{-2}$ , the LF loop dominates the spectrum when  $\alpha = 1$ . It is possible to derive an expression of the critical current densities for a given diffusion velocity from Eq. (40) and (41):

$$\alpha \neq 0.5: j_{f,crit} = \frac{4FP \ln(1 + 0.21(2\alpha - 1)) V_{diff}}{(2\alpha - 1) RT} \quad (42)$$

$$\alpha = 0.5: j_{f,crit} = 4Fc_{O_2}^* V_{diff} \quad (43)$$

The corresponding values of the critical current densities are given in Table 4.

Despite the pronounced influence of the current density on the impedance spectra in the presence of convection opposite to diffusion (Figure 6), the critical current density does not vary significantly with  $\alpha$  (less than 15%) and the values of the critical current density are quite low. This estimation of the critical current density and the impedance spectra in Figure 6 means we may understand the origin of the limiting current density in a fuel cell. At high current densities, mass transport losses become predominant and diffusion is not sufficient to transport oxygen to the reaction sites. It should be noted that the curves in Figure 6 are obtained in the case of a weakly limited diffusion in pure gas phase ( $D^{eff} = 10^{-6} \text{ m}^2 \text{ s}^{-1}$ ). In the case of higher mass diffusion limitations (diffusion in liquid phase, decreasing porosity due to liquid water accumulation, etc.), the impact of  $j_f$  on the impedance spectra would be even more significant.

## 4 Experimental Results

### 4.1 Experimental Setup

The experimental results were obtained with a single cell of active area  $A_{geom} = 23.88 \text{ cm}^2$  (Figure 7). The flow field plates were made of gold plated brass. The anode and the cathode plates were symmetrical with 28 vertical parallel channels (50 x 1 x 0.4 mm in length, width and depth). The MEA (Johnson Matthey Technologies) consisted of a 30  $\mu\text{m}$  thick PFSA (Gore) polymer membrane and Pt/C electrodes ( $\approx 10 \mu\text{m}$ ) with a platinum load of 0.2  $\text{mg}_{Pt} \text{ cm}^{-2}$  at the anode and 0.6  $\text{mg}_{Pt} \text{ cm}^{-2}$  at the cathode. The electrodes were covered with a MPL ( $\delta_{MPL} = 45 \mu\text{m}$ ) and a GDL with a hydrophobic coating of 5 wt% PTFE (SGL 10 BB,  $\delta_{GDL+MPL} = 420 \mu\text{m}$ ; Sigracet®). This cell was initially designed to study the influence of a temperature difference  $\Delta T$  between the anode and cathode plates on the water transport coefficient  $\alpha$ . Actually, the first results showed that it is possible to vary  $\alpha$  over a wide range of values (from 0.25 to 1.3) through the variation of  $\Delta T$  [28]. This enabled the measurement of the impedance spectra for different values of the water transport coefficient. Moreover, the major result of these studies is that the transport of water in the direction perpendicular to the membrane occurs like in a heat pipe in three stages:

- Evaporation under the effect of a locally higher temperature at the electrode.
- Convection and/or diffusion in the gas phase through the porous media (GDL, MPL and catalyst layer).

- And eventually, condensation in the gas channel.

A discussion of this description is not within the scope of this work (one can refer to [28]), but its consequences in term of impedance are of great interest.

The cell was operated with pure hydrogen ( $S_{H_2} = 1.4$ ) and air ( $S_{air} = 3$ ) in co-flow, at atmospheric pressure and at a mean cell temperature of  $60^\circ\text{C}$ . The gases were humidified and heated by a bubbler system. Their temperature was measured with a K-type thermocouple. Heating elements were used to avoid condensation between the outlet of the bubbler system and the cell inlet. The temperature of the flow-field plates was controlled by a water cooling system ensuring an accuracy of  $\pm 0.1^\circ\text{C}$ . The relative humidity of the gases could thus be estimated as a function of their temperature in the bubbler and the temperature of the flow-field plates. The humidification temperatures were chosen in order to obtain gases saturated with vapor and consequently,  $\alpha$  could reach values above 1 and below 0, the flux of water through the membrane being possibly negative (from the cathode to the anode) or greater than  $N_{H_2O}^{prod} = j_f / 2F$ . At the flow-field outlet the gases flowed through condensers which were maintained at  $8^\circ\text{C}$  by a Peltier element. The value of  $\alpha$  was determined by weighing the amount of water at the outlet of the condensers at each electrode.

The impedance measurements were performed in a galvanostatic mode at frequencies ranging logarithmically from 0.025 Hz to 4000 Hz with a resolution of 10 points per decade and a peak-to-peak sinusoidal perturbation of 5% of the cell current (at  $\langle j_{cell} \rangle = 0.5 \text{ Acm}^{-2}$ ,  $\Delta j_{cell} = 25 \text{ mAcm}^{-2}$  and  $\Delta V \leq 30 \text{ mV}$ ). We verified that the signal oscillations did not influence the measured impedance. Since the cell impedance is almost entirely determined by the cathode, the membrane and some contact resistances, it is possible to use the anode as a reference electrode [7]. The current collection is related to an electronic load (Amrel FEL-60-1) which is driven by a signal generator. The whole experimental setup was controlled by a Labview program.

## 4.2 Results and Discussion

Figure 8 shows impedance spectra measured at two different current densities ( $j_{cell} = 1.2 \text{ Acm}^{-2}$  and  $j_{cell} = 1.7 \text{ Acm}^{-2}$ ) for three different values of the water transport coefficient per operating point. The cell impedance increased with  $\alpha$  which is consistent with the numerical results. Inversely, it can be concluded from these curves that a convective flow in the same direction as diffusion ( $\alpha < 0.5$ ) can improve oxygen transport through the catalyst layer, which should result in better cell performances [28]. The comparison of spectra measured at  $1.2 \text{ Acm}^{-2}$  with those measured at  $1.7 \text{ Acm}^{-2}$  confirms that the impact of convection is more important at high current densities.

The experimental data measured at  $j_{cell} = 1.2 \text{ Acm}^{-2}$  were fitted (Figure 9) with the impedance expression of Eq. (20) where the oxygen transport impedance is calculated using either a classical finite Warburg element (34) (green lines) or the 1D convecto-diffusive impedance (33) (red lines). The simultaneous estimation of the 6 impedance parameters, including those of the convecto-diffusive impedance ( $R_{hf}$ ,  $R_{ct}$ ,  $C_{dl}$ ,  $D^{eff}$ ,  $\delta$  and  $\alpha$ ) is not possible, probably because  $\alpha$  is correlated with other parameters. Therefore,  $\alpha$  was determined directly by measuring the water output at the outlet of each electrode and was imposed as a fixed model parameter. The estimated impedance parameters are given in Table 5.

The data was fitted over frequencies comprised between 0.32 Hz and 200 Hz. The data beyond this frequency interval was excluded from the analysis because the impedance spectra were found to display inductive loops in the very low and high frequency domain. The values of the high frequency parameters ( $R_{hf}$ ,  $R_{ct}$ ,  $C_{dl}$ ) were typical of PEMFC [1, 37]. They were not significantly affected by the choice of the mass transport model, except for the charge transfer resistance, most probably because of correlation(s) with the faradaic current density via the oxygen concentration (2), since  $R_{ct} = b/j_f$ .

The values of the diffusion parameters ( $D^{eff}$ ,  $\delta$ ) were calculated considering the oxygen flux relative to the MEA flat surface and were also found to comply with the range which is typical of gas diffusion in PEMFC backing layers [34, 38]. The choice of the oxygen transport model modifies mostly the value of the diffusion coefficient  $D^{eff}$ . For  $\alpha = 0.25$ , the value of  $D^{eff}$  obtained with the Warburg impedance was higher than with the convecto-diffusive model, the convective flux being oriented in the same direction as diffusion. For  $\alpha = 0.7$  and  $\alpha = 1.2$  (convection opposite to diffusion) the tendency was reversed and the diffusivities estimated with the Warburg impedance were lower than with the 1D convecto-diffusive impedance. Furthermore, the difference between the values estimated with both models increases with the water transport coefficient (7% for  $\alpha = 0.7$  compared to 30% for  $\alpha = 1.2$ ). These results are consistent with our prior expectations and confirm the validity of the 1D convecto-diffusive impedance model, at least from a qualitative point of view.

The diffusion thickness  $\delta$  was less affected by the choice of the oxygen transport impedance (even for  $\alpha = 1.2$ , the relative discrepancy between both oxygen transport models does not exceed 20%). Convection can possibly impact the diffusion thickness indirectly by means of the content of liquid water present in the gas pores: when the convective flux from the cathode to the channel ( $\alpha > 0.5$ ) increases, more water is (probably) present in the porous media of the cathode. This could thus lead to an increase of the tortuosity and consequently to higher values of  $\delta$ . On the contrary, if  $\alpha$  is lower than 0.5, it is likely that there is less liquid water in the cathode (convection oriented from the air channel to the membrane). In this case, a decrease of the diffusion

thickness can be observed. The values of  $\delta$  estimated with the 1D convecto-diffusive impedance at  $1.2 \text{ Acm}^{-2}$  are consistent with this explanation. However, this is not the case for the values of  $D^{\text{eff}}$  (Table 5) since the diffusion coefficients should rather remain constant or decrease with  $\alpha$ . As the model was based on the assumption that water is evacuated in pure vapor phase, it is possible that  $V$  was overestimated; in spite of the evaporation and condensation processes in (or at the boundaries of) the porous media (heat pipe effect), some water may have been evacuated in liquid form, which is not considered here.

It should also be noted that a consistent parameter estimation was not possible for the impedance spectra measured at  $j_f = 1.7 \text{ Acm}^{-2}$ , neither with the Warburg impedance nor with the 1D convecto-diffusive impedance. This shows that these impedance models are not fully appropriate in such operating conditions and some phenomena governing the cell impedance at high current densities are not covered by the present models (possible evacuation of water in liquid phase) and/or correlations may occur between the parameters in these conditions. Nevertheless, the experimental observations confirm qualitatively the numerical results presented above.

## 5 Conclusions

The study presents a one-dimensional oxygen transport impedance model of  $\text{H}_2/\text{air}$  PEMFC, which accounts for oxygen transport by convection in addition to diffusion resulting from vapor evacuation. The convective flux was accounted for by means of the water transport coefficient  $\alpha$ . The usual description of oxygen transport leading to the Warburg impedance assumes a purely diffusive flux (and thus that  $\alpha = 0.5$ ), which is not always actually the case. The presented analytical impedance expression allows the analysis of the impact of convection perpendicular to the electrode on the oxygen concentration at the reaction interface and thus on the cell impedance spectra as a function of the operating conditions. The numerical results indicate that as long as diffusion losses are small compared to other cell voltage losses and for relatively low current densities ( $j_{\text{cell}} \leq 0.5 \text{ Acm}^{-2}$ ), convection has no significant impact on the impedance spectra. However, for higher current densities and with increasing diffusion limitations (e.g. with the appearance of liquid water in the diffusion media) the contribution of convection to the cell impedance becomes significant and should be taken into account to avoid misleading conclusions about the oxygen transport processes.

A comparison of the maximum possible current density (for a non zero oxygen concentration at the reaction interface) as a function of the water transport coefficient showed that the value of  $j_{f,\text{crit}}$  does not vary significantly with  $\alpha$  (less than 12% in the considered operating conditions). These numerical results show that at high current densities, diffusion alone does not suffice to provide oxygen supply which is an explanation for the critical current density in fuel cells.

These results are confirmed by experimental impedance spectra measured with a PEMFC single cell at different current densities. The comparison of the impedance parameters estimated using a finite Warburg impedance and the 1D convecto-diffusive impedance led us to draw the following conclusions:

- As expected, the finite Warburg impedance tends to overestimate the diffusion coefficient in the presence of a convective flux in the same direction as oxygen diffusion ( $\alpha > 0.5$ ) and to underestimate it when convection is oriented in the direction opposite to diffusion ( $\alpha < 0.5$ ).
- The discrepancy between the diffusion parameters identified with both models increases with the current density.
- At high current densities, a consistent parameter estimation is not possible. This could result from correlations between the model parameters or by phenomena not considered in the 1D convecto-diffusive impedance, like evacuation of water in liquid phase. This is certainly the model's most important shortcoming.
- It should also be noted finally that the values of  $D^{\text{eff}}$  and  $\delta$  estimated with both transport models do not vary drastically. At moderate current densities and for a first estimation of the diffusion parameters, convection perpendicular to the electrode can be neglected. This is consistent with the results of the numerical investigations.

## List of Symbols

Latin letters

A	MEA surface / $\text{cm}^2$
b	Tafel slope / mV
c	Concentration / $\text{mol cm}^{-3}$
C	Capacity / $\text{Fcm}^{-2}$
D	Binary diffusion coefficient / $\text{m}^2\text{s}^{-1}$
E	Voltage / V
F	Faraday's constant / $F=96485 \text{ Cmol}^{-1}$
j	Current density / $\text{Acm}^{-2}$
J	Diffusive flux density / $\text{mol m}^{-2}\text{s}^{-1}$
N	Gas flux density / $\text{mol m}^{-2}\text{s}^{-1}$

P	Pressure / bar
R	Gas constant / $8.314 \text{ J mol}^{-1}\text{K}^{-1}$ , Resistance/ $\Omega\text{cm}^2$
T	Temperature / K
V	Flux velocity (convective) / $\text{ms}^{-1}$
Z	Impedance / $\Omega\text{cm}^2$
Greek letters	
$\alpha$	Water transport coefficient
$\delta$	Diffusion layer thickness / $\mu\text{m}$
$\varepsilon$	Porosity
$\eta$	Overpotential / V
$\nu$	Frequency / Hz
$\omega$	Angular frequency / $\text{rad}^{-1}$
Super scripts	
*	Equilibrium
conv	Convective
eff	Effective
GDL	Backing layers
MPL	Micro porous layer
prod	Produced
tot	Total
Sub scripts	
0	Open circuit / Exchange
act	Activation
c	Capacitive / Concentration
cell	Cell
conv	Convective
crit	Critical
ct	Charge transfer
diff	Diffusive
dl	Double layer
f	Faradaic
geom	Geometrical (flat)
H <sub>2</sub>	Hydrogen
H <sub>2</sub> O	Water
hf	High frequency
lf	Low frequency
lim	Limit
O <sub>2</sub>	Oxygen
W	Warburg

## References

- [1] T. Springer, T. Zawodzinski, M. Wilson, S. Gottesfeld, *J. Electrochem. Soc.* **1996**, *143*, 587.
- [2] V. Paganin, C. Oliveira, E. Ticianelli, T. Springer, E. Gonzalez, *Electrochim. Acta* **1998**, *43*, 3761.
- [3] T. Okada, G. Xie, Y. Tanabe, *J. Electroanal. Chem.* **1996**, *413*, 49.
- [4] T. Springer, I. Raistrick, *J. Electrochem. Soc.* **1989**, *136*, 1594.
- [5] I. Raistrick, *Electrochim. Acta* **1990**, *35*, 1579.
- [6] O. Antoine, Y. Bultel, R. Durand, *J. Electroanal. Chem.* **2001**, *499*, 85.
- [7] M. Ciureanu, R. Roberge, *J. Phys. Chem. B* **2001**, *105*, 3531.
- [8] N. Wagner, *J. Appl. Electrochem.* **2002**, *32*, 859.
- [9] S. Lee, S. Mukerjee, J. McBreen, Y. Rho, Y. Kho, T. Lee, *Electrochim. Acta* **1998**, *43*, 3693.
- [10] Y. Bultel, L. Genies, O. Antoine, P. Ozil, R. Durand, *J. Electroanal. Chem.* **2002**, *527*, 143.
- [11] Y. Bultel, K. Wiezell, F. Jaouen, P. Ozil, G. Lindbergh, *Electrochim. Acta* **2005**, *51*, 474.
- [12] S. Nakamura, H. Nishikawa, T. Aoki, Y. Ogami, *J. Power Sources* **2009**, *186*, 278.
- [13] I. Schneider, D. Kramer, A. Wokaun, G. Scherer, *J. Electrochem. Soc.* **2007**, *154*, B770.
- [14] I. Schneider, S. Freunberger, D. Kramer, A. Wokaun, G. Scherer, *J. Electrochem. Soc.* **2007**, *154*, B383.
- [15] D. R. Franceschetti, J. Macdonald, R. P. Buck, *J. Electrochem. Soc.* **1991**, *138*, 1368.
- [16] V. Freger, *Electrochem. Commun.* **2005**, *7*, 957.
- [17] D. Kramer, I. A. Schneider, A. Wokaun, G. G. Scherer, *ECS Trans.* **2006**, *3*, 1249.
- [18] J. P. Diard, B. Le Gorrec, C. Montella, C. Poinson, G. Vitter, *J. Power Sources* **1998**, *74*, 244.

- [19] E. Passalacqua, G. Squadrito, F. Lufrano, A. Patti, L. Giorgi, *J. Appl. Electrochem.* **2001**, *31*, 449.
- [20] J. Itonen, M. Mikkola, G. Lindbergh, *J. Electrochem. Soc.* **2004**, *151*, A1152.
- [21] N. Wagner, W. Schnurnberger, B. Müller, M. Lang, *Electrochim. Acta* **1998**, *43*, 3785.
- [22] M. Eikerling, A. Kornyshev, *J. Electroanal. Chem.* **1999**, *475*, 107.
- [23] T. Springer, M. Wilson, S. Gottesfeld, *J. Electrochem. Soc.* **1993**, *140*, 3513.
- [24] J. Deseure, *J. Power Sources* **2008**, *178*, 323.
- [25] M. Bayer, A. Wokaun, G. Scherer, I. Schneider, *ECS Transactions* **2009**, *25*, 949.
- [26] S. Devan, V. Subramanian, R. White, *J. Electrochem. Soc.* **2004**, *151*, A905.
- [27] E. Warburg, *Annalen der Physik und Chemie* **1899**, *69*, 493.
- [28] A. Thomas, G. Maranzana, S. Didierjean, O. Lottin, J. Dillet, A. Lamibrac, *Proceedings of the Fundamentals and Developments of Fuel Cells Conference 2011*, 19th-21st January 2011, Grenoble, France, **2011**.
- [29] S. Chupin, T. Colinart, S. Didierjean, Y. Dubé, K. Agbossou, G. Maranzana, O. Lottin, *J. Power Sources* **2010**, *195*, 5213.
- [30] J. Mainka, G. Maranzana, J. Dillet, S. Didierjean, O. Lottin, *J. Electrochem. Soc.* **2010**, *157*, B1561.
- [31] S. Torquato, *Random Heterogeneous Materials: Microstructure and Macroscopic Properties*, Springer, **2002**.
- [32] G. Archie, *Trans. AIME* **1942**, *146*, 54.
- [33] P. Argyropoulos, K. Scott, W. Taama, *J. Appl. Electrochem.* **1999**, *29*, 661.
- [34] R. Bird, W. Stewart, E. Lightfoot, *Transport Phenomena*, John Wiley and Sons, New York, **2002**.
- [35] R. Krishna, J. Wesselingh, *Chem. Eng. Sci.* **1997**, *52*, 861.
- [36] T. Colinart, A. Chenu, S. Didierjean, O. Lottin, S. Besse, *J. Power Sources* **2009**, *190*, 230.
- [37] M. Rubio, A. Urquia, R. Kuhn, S. Dormido, *J. Power Sources* **2008**, *183*, 118.
- [38] J. Gostick, M. Fowler, M. Pritzker, M. Ioannidis, L. Behra, *J. Power Sources* **2006**, *162*, 228.

## Figure Caption

Fig. 1 One-dimensional convecto-diffusive mass transport model.

Fig. 2 Normalized oxygen concentration at the membrane/GDL interface ( $x=0$ ) for three different values of the water transport coefficient: a purely diffusive flux ( $\alpha=0.5$ ; in red), and with an additional convective flux in the same direction ( $\alpha=0$ ; in black) or in the opposite direction ( $\alpha=1$ ; in blue).

Fig. 3 Normalized discrepancy  $\Delta c_{O_2}^\alpha(0) = \left| c_{O_2}^{\alpha=0.5}(0) - c_{O_2}^\alpha(0) \right|$  between the oxygen concentration at the reaction interface with a purely diffusive flux ( $\alpha=0.5$ ) and with a convecto-diffusive flux in the two limit cases ( $\alpha=0,1$ ) as a function of the current density.

Fig. 4 Impedance spectra simulated in the conditions of Table 1 for different values of  $R_{ct}$  (a) and  $C_{dl}$  (b).

Fig. 5 Impedance spectra simulated in the conditions of Table 1 for different values of (a) the effective diffusivity  $D^{eff}$  and of (b) the diffusion layer thickness  $\delta$ . The impact of the convection becomes more pronounced with increasing  $\delta$  or decreasing  $D^{eff}$  (i.e. with decreasing diffusion velocity  $V_{diff} = \delta/D^{eff}$ ).

Fig. 6 Impedance spectra simulated in the conditions of Table 1 for different values of the current density: (a) low current densities ( $0.5 \text{ Acm}^{-2}$  and  $1 \text{ Acm}^{-2}$ ); (b)  $j_f = 1.3 \text{ Acm}^{-2}$ . The effect of convection increases with the current density.

Fig. 7 Flow field plates (gold plated brass; the anode and the cathode plates are symmetrical with 28 parallel channels) and MEA (Johnson Matthey Technologies;  $A_{geom} = 23.88 \text{ cm}^2$ ) of the single cell used for experimental studies.

Fig. 8 Impedance spectra measured with the single cell of Figure 7 (open dots:  $j_{cell} = 1.2 \text{ Acm}^{-2}$ ; triangles:  $j_{cell} = 1.7 \text{ Acm}^{-2}$ ) for different values of the water transport coefficient.  $\alpha$  is controlled by the temperature difference between the anode and the cathode flow field plates.

Fig. 9 Impedance spectra of Figure 8 at  $j_{cell} = 1.2 \text{ Acm}^{-2}$  with corresponding fitting curves obtained using a Randles EEC with different models of the oxygen transport impedance: the finite Warburg impedance (green lines) and the 1D convecto-diffusive impedance (red lines).

## Tables

Table 1 Reference values used for the impedance analysis.

Working conditions:	T	[°C]	60
	P	[bar]	1
	$j_f$	[ $\text{Acm}^{-2}$ ]	0.5

Mass transport characteristics:	$\delta$	[ $\mu\text{m}$ ]	200
	$D^{\text{eff}}$	[ $\text{m}^2\text{s}^{-1}$ ]	$10^{-6}$
Impedance parameters:	$R_{\text{hf}}$	[ $\Omega\text{cm}^2$ ]	0.13
	$R_{\text{ct}}$	[ $\Omega\text{cm}^2$ ]	0.19
	$B$	[mV]	95
	$C_{\text{dl}}$	[ $\text{Fcm}^{-2}$ ]	0.02

Table 2 Numerical values of  $\Delta Z_{\text{CO}_2}^\alpha$  and  $\Delta R_{\text{lf}}^\alpha$  calculated in the conditions of Table 1.

$V_{\text{diff}}$ [ $\text{ms}^{-1}$ ]	$\alpha$ [-]	$\Delta Z_{\text{CO}_2}^\alpha$ [%]	$\Delta R_{\text{lf}}^\alpha$ [%]
$5 \cdot 10^{-3}$	0	20	5
	1	19	4
$2.5 \cdot 10^{-3}$	0	26	15
	1	35	19

Table 3 Critical values of the diffusion parameters (for which the oxygen concentration at the GDL/membrane interface becomes zero) in the conditions of the reference case in Table 1. The critical effective diffusivity

$D_{\text{crit}}^{\text{eff}}$  is calculated with  $\delta = 200 \mu\text{m}$  and the critical diffusion layer thickness  $\delta_{\text{crit}}$  with  $D_{\text{eff}} = 10^{-6} \text{m}^2\text{s}^{-1}$ .

$\alpha$ [-]	$V_{\text{diff}}^{\text{crit}}$ [ $\text{ms}^{-1}$ ]	$D_{\text{crit}}^{\text{eff}}$ [ $\text{m}^2\text{s}^{-1}$ ]	$\delta_{\text{crit}}$ [ $\mu\text{m}$ ]
0	$4.63 \cdot 10^{-4}$	$3.04 \cdot 10^{-7}$	657
0.5	$5.84 \cdot 10^{-4}$	$3.42 \cdot 10^{-7}$	586
1	$7.07 \cdot 10^{-4}$	$3.76 \cdot 10^{-7}$	532

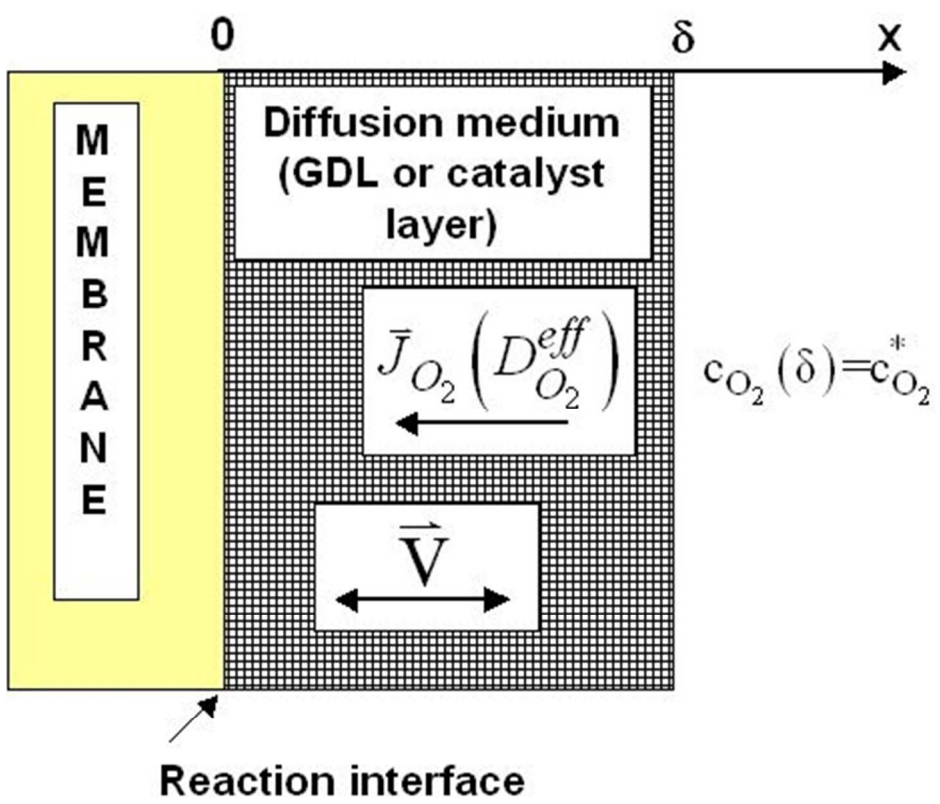
Table 4 Critical current densities in the operating conditions of Table 1.

$\alpha$ [-]	$j_{\text{c,crit}}$ [ $\text{Acm}^{-2}$ ]	$V$ [ $\text{ms}^{-1}$ ]
0	1.64	$-1.2 \cdot 10^{-3}$
0.5	1.46	0
1	1.33	$1 \cdot 10^{-3}$

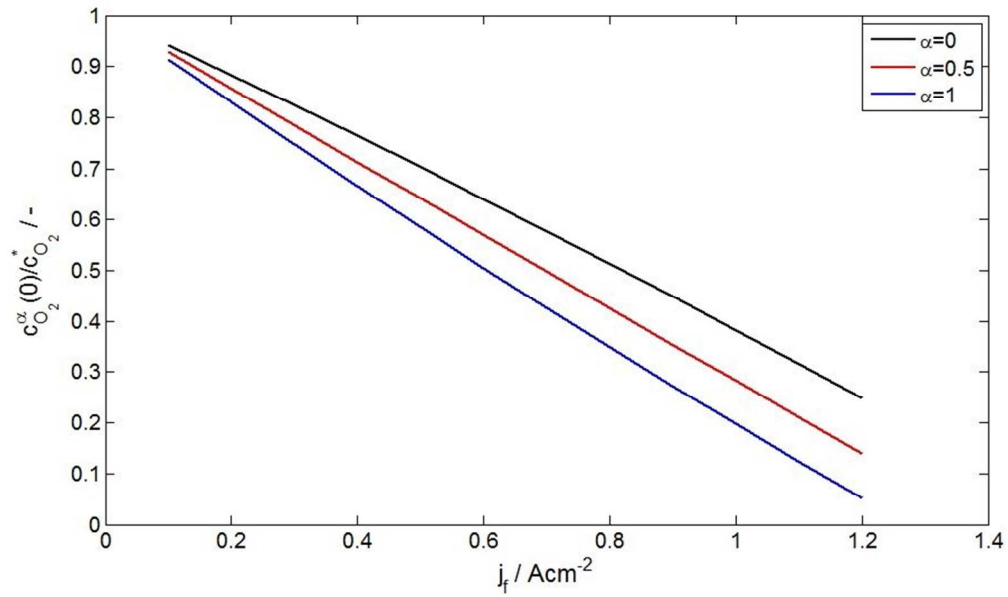
Table 5 Impedance parameters identified from the impedance spectra of Figure 9; at  $j_{\text{cell}}=1.2 \text{Acm}^{-2}$ .

	$\alpha$	$R_{\text{hf}}$	$R_{\text{ct}}$	$C_{\text{dl}}$	$D^{\text{eff}}$	$\delta$
	[-]	[ $\Omega\text{cm}^2$ ]	[ $\Omega\text{cm}^2$ ]	[ $\text{Fcm}^{-2}$ ]	[ $\text{m}^2\text{s}^{-1}$ ]	[ $\mu\text{m}$ ]
Warburg		0.194	0.176	0.016	$2.05 \cdot 10^{-6}$	354
Conv-diff 1D	0.25	0.195	0.180	0.016	$1.83 \cdot 10^{-6}$	329
Warburg		0.187	0.179	0.018	$1.97 \cdot 10^{-6}$	363
Conv-diff 1D	0.7	0.186	0.174	0.018	$2.13 \cdot 10^{-6}$	383
Warburg		0.185	0.182	0.019	$2.01 \cdot 10^{-6}$	374
Conv-diff 1D	1.2	0.184	0.163	0.019	$2.61 \cdot 10^{-6}$	447

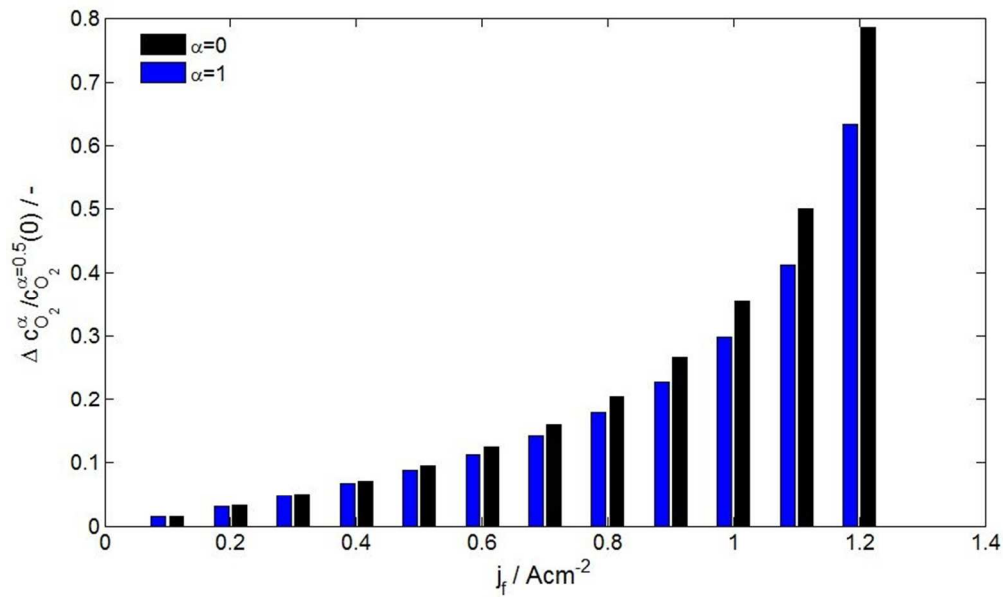
1  
2  
3  
4  
5  
6  
7  
8  
9  
10  
11  
12  
13  
14  
15  
16  
17  
18  
19  
20  
21  
22  
23  
24  
25  
26  
27  
28  
29  
30  
31  
32  
33  
34  
35  
36  
37  
38  
39  
40  
41  
42  
43  
44  
45  
46  
47  
48  
49  
50  
51  
52  
53  
54  
55  
56  
57  
58  
59  
60



One-dimensional convecto-diffusive mass transport model.  
125x108mm (96 x 96 DPI)

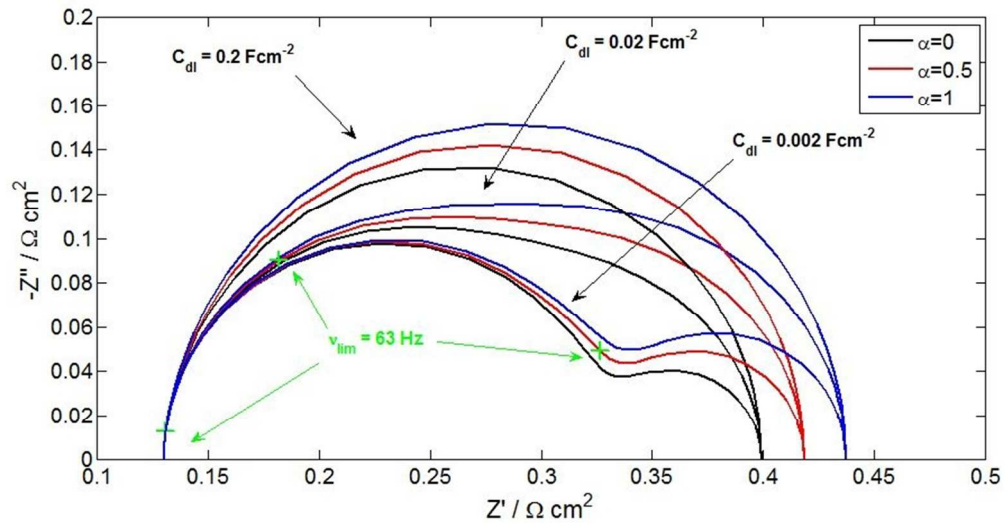


Normalized oxygen concentration at the membrane/GDL interface ( $x=0$ ) for three different values of the water transport coefficient: a purely diffusive flux ( $\alpha=0.5$ ; in red), and with an additional convective flux in the same direction ( $\alpha=0$ ; in black) or in the opposite direction ( $\alpha=1$ ; in blue).  
237x141mm (96 x 96 DPI)

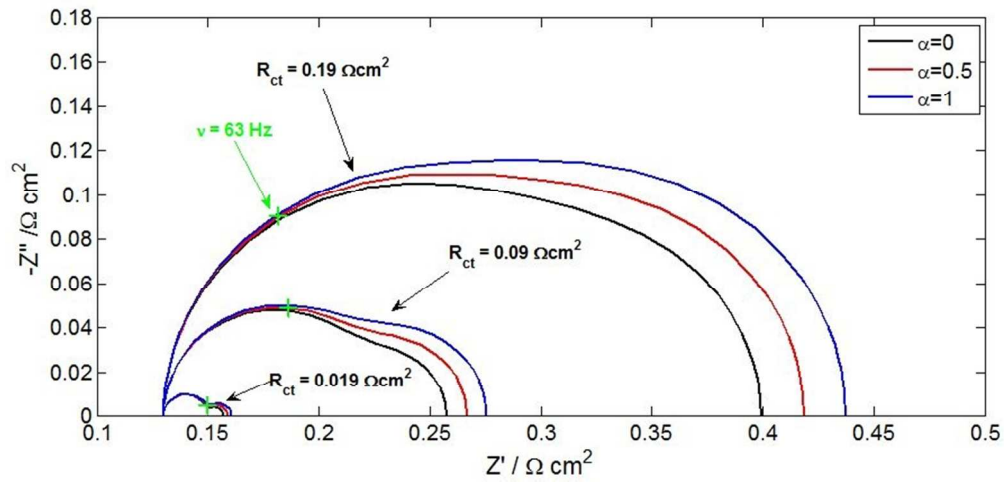


Normalized discrepancy between the oxygen concentration at the reaction interface with a purely diffusive flux ( $\alpha = 0.5$ ) and with a convecto-diffusive flux in the two limit cases ( $\alpha=0,1$ ) as a function of the current density.

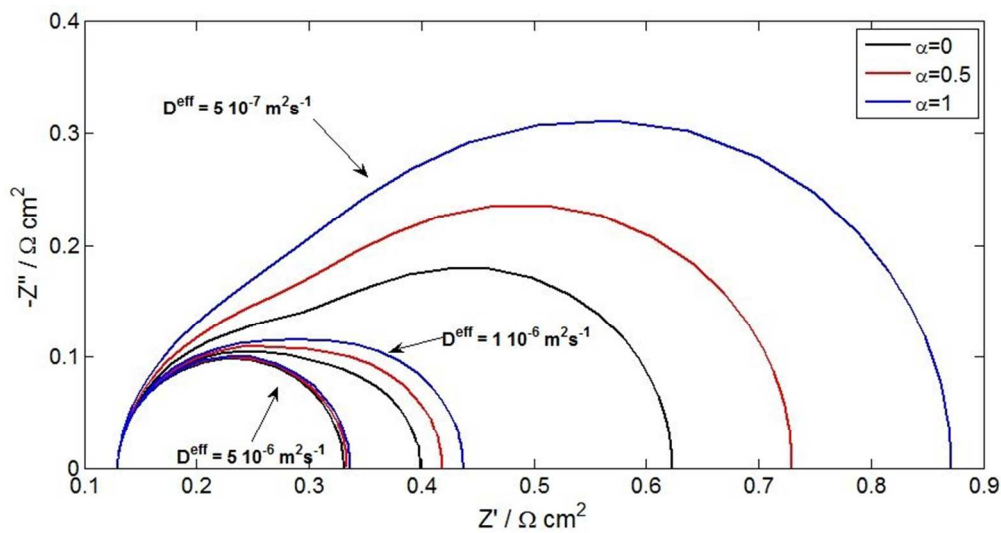
237x142mm (96 x 96 DPI)



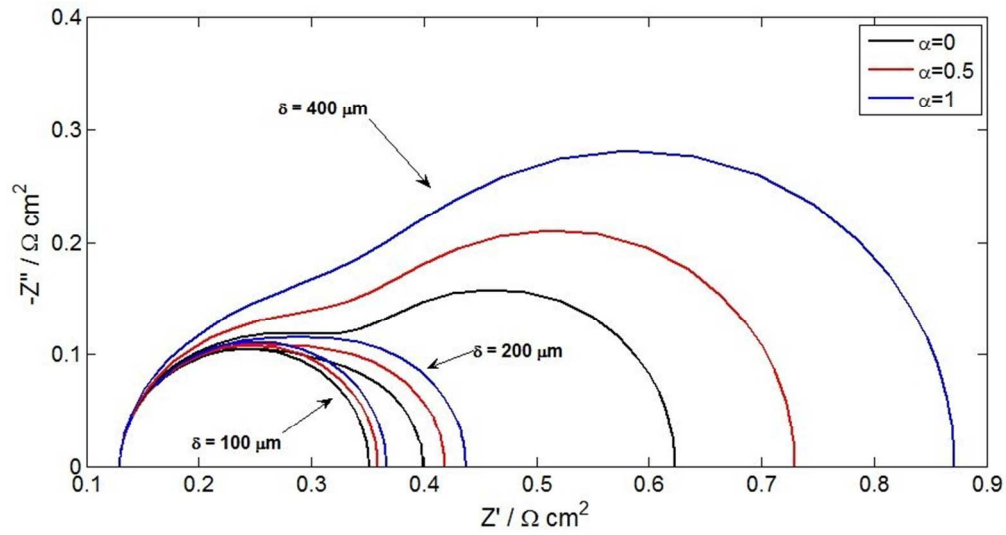
Impedance spectra simulated in the conditions of Table 1 for different values of  $R_{ct}$  (a) and  $C_{dl}$  (b).  
235x123mm (96 x 96 DPI)



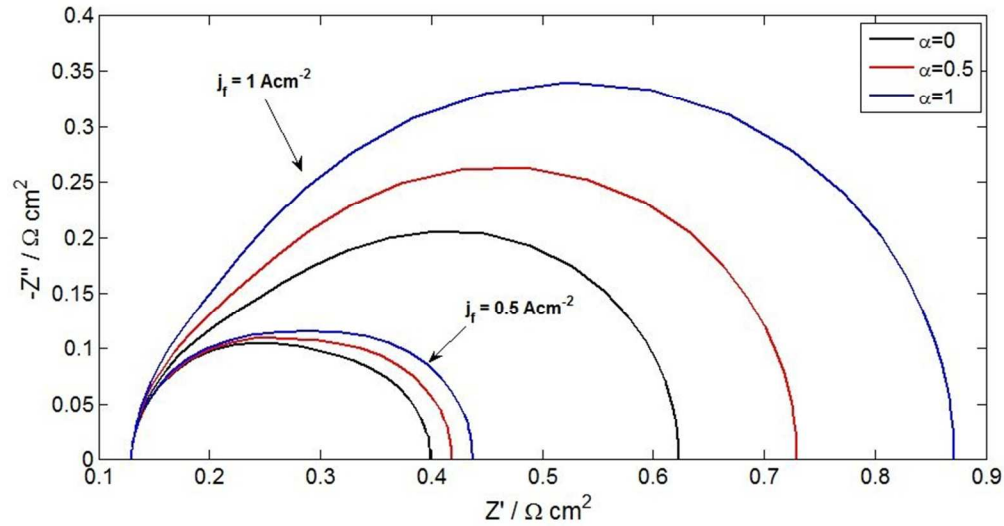
Impedance spectra simulated in the conditions of Table 1 for different values of  $R_{ct}$  (a) and  $C_{dl}$  (b).  
235x114mm (96 x 96 DPI)



Impedance spectra simulated in the conditions of Table 1 for different values of (a) the effective diffusivity  $D^{\text{eff}}$  and of (b) the diffusion layer thickness  $\delta$ . The impact of the convection becomes more pronounced with increasing  $\delta$  or decreasing  $D^{\text{eff}}$  (i.e. with decreasing diffusion velocity  $V_{\text{diff}} = \delta/D^{\text{eff}}$ ).  
232x123mm (96 x 96 DPI)

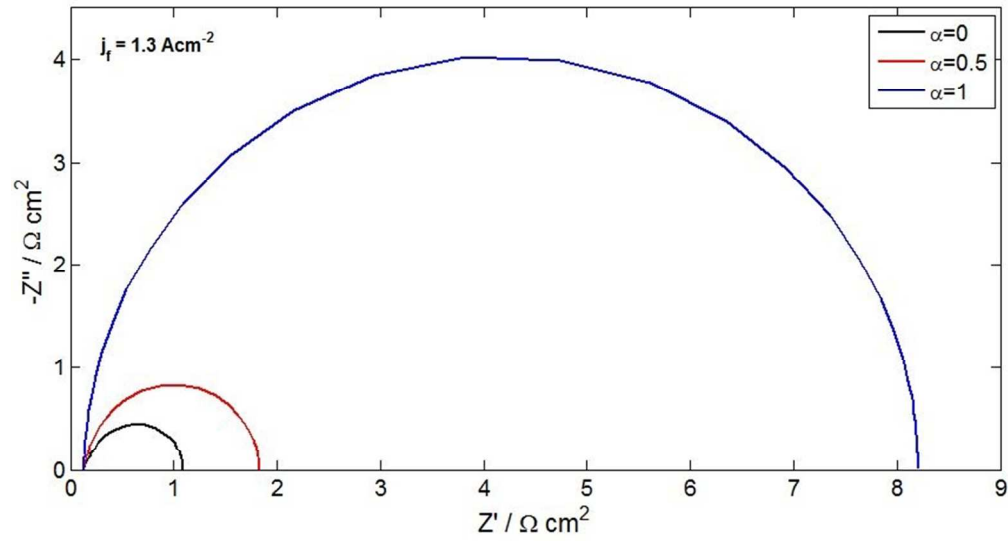


Impedance spectra simulated in the conditions of Table 1 for different values of (a) the effective diffusivity  $D_{\text{eff}}$  and of (b) the diffusion layer thickness  $\delta$ . The impact of the convection becomes more pronounced with increasing  $\delta$  or decreasing  $D_{\text{eff}}$  (i.e. with decreasing diffusion velocity  $V_{\text{diff}} = \delta/D_{\text{eff}}$ ).  
232x123mm (96 x 96 DPI)



Impedance spectra simulated in the conditions of Table 1 for different values of the current density: (a) low current densities ( $0.5 \text{ Acm}^{-2}$  and  $1 \text{ Acm}^{-2}$ ); (b)  $j_f = 1.3 \text{ Acm}^{-2}$ . The effect of convection increases with the current density.

235x126mm (96 x 96 DPI)



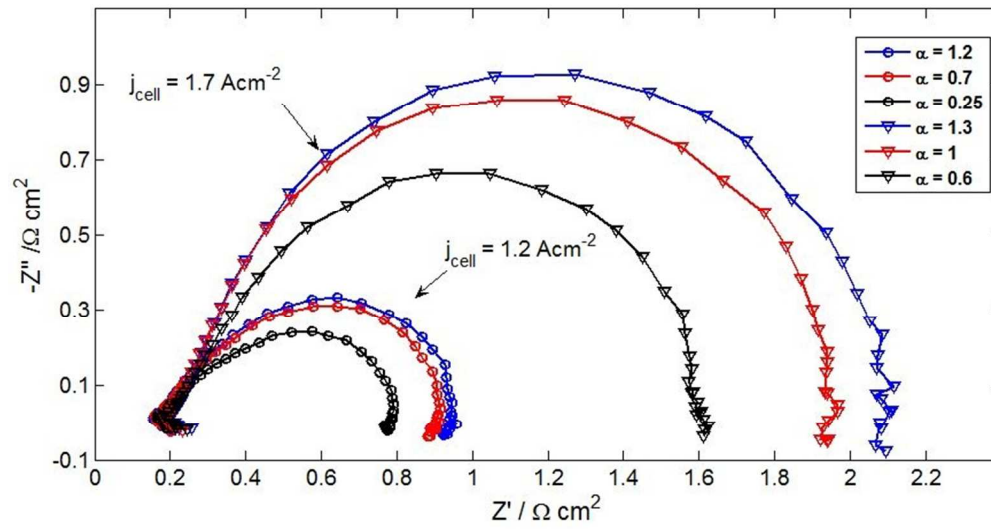
25 Impedance spectra simulated in the conditions of Table 1 for different values of the current density: (a) low  
26 current densities (0.5 Acm<sup>-2</sup> and 1 Acm<sup>-2</sup>); (b) j<sub>r</sub> = 1.3 Acm<sup>-2</sup>. The effect of convection increases with the  
27 current density.

28 225x121mm (96 x 96 DPI)

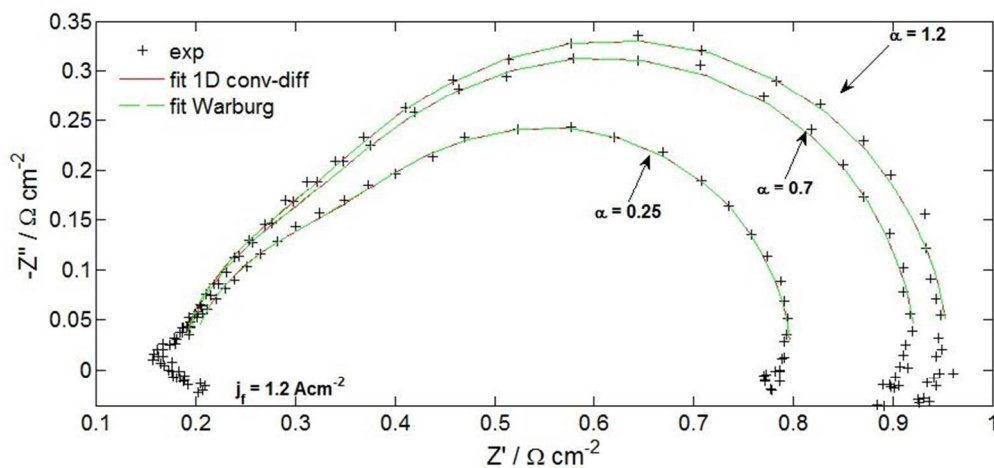


Flow field plates (gold plated brass; the anode and the cathode plates are symmetrical with 28 parallel channels) and MEA (Johnson Matthey Technologies; Ageom = 23.88 cm<sup>2</sup>) of the single cell used for experimental studies.  
214x80mm (72 x 72 DPI)

Peer Review



Impedance spectra measured with the single cell of Figure 7 (open dots:  $j_{\text{cell}} = 1.2 \text{ Acm}^{-2}$ ; triangles:  $j_{\text{cell}} = 1.7 \text{ Acm}^{-2}$ ) for different values of the water transport coefficient.  $\alpha$  is controlled by the temperature difference between the anode and the cathode flow field plates.  
230x122mm (96 x 96 DPI)



Impedance spectra of Figure 8 at  $j_{\text{cell}} = 1.2 \text{ A cm}^{-2}$  with corresponding fitting curves obtained using a Randles EEC with different models of the oxygen transport impedance: the finite Warburg impedance (green lines) and the 1D convecto-diffusive impedance (red lines).  
233x109mm (96 x 96 DPI)